

22 **Abstract**

23 Atmospheric models often underestimate particulate sulfate, a major component in ambient
24 aerosol, suggesting missing sulfate formation mechanisms in the models. Heterogeneous
25 reactions between SO₂ and aerosol play an important role in particulate sulfate formation and its
26 physicochemical evolution. Here we study the reactive uptake kinetics of SO₂ onto aerosol
27 containing organic peroxides. We present chamber studies of SO₂ reactive uptake performed
28 under different relative humidities (RH), particulate peroxide contents, peroxide types, and
29 aerosol acidities. Using different model organic peroxides mixed with ammonium sulfate
30 particles, SO₂ uptake coefficient (γ_{SO_2}) was found to be exponentially dependent on RH. γ_{SO_2}
31 increases from 10⁻³ at RH 25% to 10⁻² at RH 71% as measured for an ~~an~~-multifunctional-organic
32 peroxide with multiple O-O groups. Under similar conditions, the kinetics in this study were
33 found to be structurally dependent: ~~multifunctional~~-organic peroxides with multiple peroxide
34 groups have a higher γ_{SO_2} than those with only one peroxide group, consistent with the reactivity
35 trend observed previously in the aqueous phase. In addition, γ_{SO_2} is linearly related to particle-
36 phase peroxide content, which in turn depends on gas-particle partitioning of organic peroxides.
37 Aerosol acidity plays a complex role in determining SO₂ uptake rate, influenced by the effective
38 Henry's Law constant of SO₂ and the condensed phase kinetics of the peroxide-SO₂ reaction in
39 the highly concentrated aerosol phase. These uptake coefficients are consistently higher than
40 those calculated from the reaction kinetics in the bulk aqueous phase, and we show experimental
41 evidence suggesting that other factors, such as particle-phase ionic strength, can play an essential
42 role in determining the uptake kinetics. γ_{SO_2} for different types of secondary organic aerosol
43 (SOA) were measured to be on the order of 10⁻⁴. Overall, this study provides quantitative

44 evidence of the multiphase reactions between SO₂ and organic peroxides, highlighting the
45 important factors that govern the uptake kinetics.

46 **Introduction**

47 Sulfate and organic compounds are ubiquitous particulate components in both polluted and
48 pristine environments (Chen et al., 2009;Andreae et al., 2018;He et al., 2011;Sun et al.,
49 2013;Huang et al., 2014), with important implications for public health and global climate
50 (Hallquist et al., 2009). Particulate sulfate can form via S(IV) oxidation by OH radicals in the gas
51 phase and via oxidation in cloud water, fog droplets or the aerosol aqueous phase, including by
52 H₂O₂, O₂ (catalyzed by transition metals), O₃, NO₂ and small organic peroxides (methyl
53 hydroperoxide and peroxyacetic acid) (Seinfeld and Pandis, 2012). However, atmospheric
54 models tend to underestimate particulate sulfate production on both global (Tie et al., 2001;Yang
55 et al., 2017;Fairlie et al., 2010) and regional scales, especially during heavy haze episodes (Wang
56 et al., 2014;Zheng et al., 2015;Sha et al., 2019;Gao et al., 2016;Li et al., 2017;Huang et al.,
57 2019), suggesting that the overall kinetics may be underestimated and/or important mechanisms
58 may be missing in models.

59 To reconcile these differences, studies have investigated novel reaction mechanisms of sulfate
60 formation. Stabilized Criegee intermediates (sCIs) were ~~hypothesized~~found to oxidize SO₂
61 rapidly and ~~proposed to be~~potentially serve as an important source of ambient sulfate (Mauldin et
62 al., 2012). In the work by Newland et al. (2015) and Nguyen et al. (2016), this sCIs pathway was
63 shown to play a minor role in sulfate formation. More recently, when Liu et al. (2019) applied
64 this mechanism and kinetics to a source-oriented WRF-Chem model, the sCIs pathway was
65 found to only account for at most 9% of the total particulate sulfate. Reactive nitrogen species
66 (such as NO₂) have also been put forward to account for the missing sulfate at relatively high

67 aerosol pH (close to 7) (Wang et al., 2016;Cheng et al., 2016). However, such high aerosol pH is
68 not substantiated by thermodynamic models, which conclude that pH ranges between 4 and 5
69 even in polluted regions (Song et al., 2018;Guo et al., 2017). A recent modeling study
70 incorporating this heterogeneous NO_x mechanism still exhibited a discrepancy of 20% between
71 the predicted and observed sulfate, indicating the possibility of unknown mechanisms (Huang et
72 al., 2019). Other factors may play a role in enhancing the particle-phase sulfate formation rates.
73 Chen et al. (2019) investigated the synergistic effects of NO₂ and NH₃ on sulfate formation, and
74 found that the rate of this reaction can be enhanced by the high ionic strength in the particle
75 phase. This enhancement effect by solute strength on sulfate formation was also investigated for
76 the H₂O₂ pathway in aerosol liquid water. Liu et al. (2020) found ionic strength and general acid-
77 catalyzed mechanisms can cause the S(VI) formation rate to be nearly 50 times faster in aerosol
78 phase than in dilute solutions. On the other hand, during the severe haze episodes in China (Li et
79 al., 2020; Guo et al., 2017), transition metal ion (TMI) catalysis of SO₂ oxidation by O₂ can be
80 significantly suppressed in the aerosol phase due to high ionic strength (Liu et al., 2020;Cheng et
81 al., 2016; Su et al., 2020).

82 In addition to high solute strength, submicron aerosol is also rich in organic compounds (Jimenez
83 et al., 2009;Hallquist et al., 2009). In recent years, many studies have investigated the potential
84 role of heterogeneous interactions between SO₂ and organic aerosol on particulate sulfate
85 formation. Song et al. (2019) found heterogeneous oxidation of hydroxymethanesulfonate
86 (HMS) by OH can trigger rapid sulfate formation. Wang et al. (2020) studied photosensitizers in
87 ambient particles and found this pathway could be essential under specific light conditions.
88 Recent studies found reactive intermediates from isoprene oxidation (Huang et al., 2019) and
89 benzoic acid (Huang et al., 2020), can yield a variety of organosulfur species upon catalysis by

90 TMI. Other studies have also investigated the interactions between secondary organic aerosol
91 (SOA) and SO₂. Field observations found that ambient sulfate abundance is highly correlated
92 with SOA formation (Yee et al., 2020; Xu et al., 2015). Liu et al. (2019) found that SO₂ enhances
93 SOA formation and average carbon oxidation state during methoxyphenol photooxidation. By
94 performing chamber experiments with limonene SOA formation in the presence of SO₂, Ye et al.
95 (2018) also observed significant SO₂ decay along with increased SOA yields and carbon
96 oxidation state, proposing that organic peroxides in SOA may be the key reactive intermediates
97 for SO₂ oxidation.

98 Organic peroxides are key intermediates for aerosol formation and ubiquitously exist in many
99 SOA systems (Hallquist et al., 2009; Bianchi et al., 2019). Numerous studies have reported
100 peroxide content of 20-60% for isoprene and monoterpene derived SOA (Surratt et al., 2006; Ng
101 et al., 2008; Ye et al., 2018; Epstein et al., 2014). A significant fraction of organic peroxide (30%-
102 50%) has also been found in naphthalene-derived SOA under low/high NO_x conditions
103 (Kautzman et al., 2009). Using model simulations, Bonn et al. (2004) found organic
104 hydroperoxides can account for up to 60% of global SOA. The aqueous phase reaction kinetics
105 between organic peroxides and dissolved SO₂ have been explored in previous studies (Lind et al.,
106 1987; Gunz and Hoffmann, 1990; Wang et al., 2019; Dovrou et al., 2019; Yao et al., 2019). The
107 second order reaction rate constants for organic peroxides in SOA (Dovrou et al., 2019; Yao et
108 al., 2019) and S(IV) were measured to be on the order of 10²-10³ M⁻¹ s⁻¹, which are within the
109 range of those measured for commercially available organic peroxides (Wang et al., 2019) and
110 small organic peroxides (Lind et al., 1987). Yao et al. (2019) quantified the reactive uptake
111 coefficient of SO₂ (γ_{SO_2}) onto α -pinene SOA to be on the order of 10⁻⁴-10⁻³, which is positively
112 dependent on RH and inferred particle-phase peroxide content. These reactions are also linked to

113 the formation of organosulfates (Wang et al., 2019). Both inorganic sulfate (85-90%) and
114 organosulfates (10-15%) were observed as products of SO₂ reactive uptake onto SOA (Yao et al.,
115 2019).

116 Given the potential significance of SO₂ reactive uptake in particulate sulfate formation, a more
117 in-depth study is needed to determine the important factors that govern the heterogeneous
118 kinetics of SO₂ onto organic peroxide containing aerosol. In this study, we measured γ_{SO_2} for two
119 categories of aerosol: 1. Model organic peroxides mixed with ammonium sulfate or malonic acid
120 and 2. SOA from a few representative biogenic and anthropogenic precursors. The impacts of
121 RH, peroxide type, peroxide content, and condensed phase pH on SO₂ reactive uptake were
122 evaluated systematically with the goal of better understanding atmospheric multiphase sulfate
123 formation.

124

125 **2. Methods**

126 The reactive uptake of SO₂ onto peroxide-containing particles was studied in a 1 m³ Teflon
127 chamber under ambient temperature and pressure. In brief, generated particles and SO₂ were
128 introduced into the chamber separately. The consumption of SO₂, changes in particle size
129 distribution and chemical composition were monitored to estimate the reactive uptake
130 coefficients. Particles were also collected on filters for offline chemical characterization.

131

132 **2.1 Seed aerosol generation**

133 In this work, two types of aerosol were used to investigate the uptake of SO₂. The first is
134 ammonium sulfate or malonic acid mixed with model organic peroxides (Fig. S1). In this first set
135 of experiments, an aerosol atomizer (Model 3076, TSI Inc., USA) was used to generate aqueous

136 particles from dilute solution. Each solution consists of ammonium sulfate ($\geq 99\%$, Sigma-
137 Aldrich) or malonic acid (99%, Sigma-Aldrich) and a model organic peroxide in ultrapure water
138 (HPLC grade, Fisher Chemical). For the experiments investigating the relationship between γ_{SO_2}
139 and peroxide type (Expt. 2-14, [Table S1](#)), different commercially available organic peroxides
140 were used, including tert-butyl hydroperoxide (70 wt. % in water, Sigma-Aldrich), cumene
141 hydroperoxide (80 wt. % in water, Sigma-Aldrich), and 2-butanone peroxide (40% wt. % in
142 water, Sigma-Aldrich). The molar ratio of organic peroxide to ammonium sulfate in the
143 atomizing solution was 2:1 with the aim of being atmospherically relevant (corresponding to
144 maximum particulate peroxide molar fraction of 66% and mass fraction of approximately 50-
145 70% if all the organic peroxides were assumed to remain in the particle phase). This ratio was
146 used as a proxy for total peroxide content in both gas and particle phase relative to that of
147 ammonium sulfate upon atomization. For the experiments studying the relationship between γ_{SO_2}
148 and particle-phase peroxide content, the molar ratio of organic peroxide to ammonium sulfate
149 (Expt. 10-12, 15-18, [Table S1](#)) in the solution was adjusted to be 0.02, 0.2, 1, 2, and 4,
150 respectively. In experiments where malonic acid was used (Expt. 19-22, [Table S1](#)), molar ratios
151 of 0.2, 1, 2, and 4 were adopted. For measuring γ_{SO_2} with different aerosol pH (Expt. 17, 23-25, [Table S1](#)),
152 different amounts of HCl (37%, Sigma-Aldrich) were added into the solution ([0,](#)
153 [0.00002 M, 0.0001 M, 0.001 M HCl](#)) prior to atomization. [The initial pH of aerosol \(2.5, 2.2,](#)
154 [1.6, 1, respectively\) were modeled using E-AIM III model \(Clegg et al., 1998\) based on the](#)
155 [initial molar ratios of inorganic species \(\$\text{H}^+\$, \$\text{NH}_4^+\$, \$\text{SO}_4^{2-}\$, \$\text{Cl}^-\$ \) in the atomizing solution and](#)
156 [measured RH \(around 50%\).](#) The atomized particles were flowed into the chamber without
157 drying, and therefore assumed to remain deliquesced under the range of RH we studied. Expt. 2-

Formatted: Superscript

Formatted: Subscript

Formatted: Superscript

Formatted: Subscript

Formatted: Superscript

Formatted: Superscript

158 14 (Table S1) also represent those where the relationship between γ_{SO_2} and RH conditions were
159 studied.

160 In the second set of experiments, the uptake of SO_2 onto SOA was investigated (Fig. S2, Expt.
161 26-28, Table S1). A custom-built 10 L quartz oxidation flow reactor was used to produce SOA
162 (Ye et al., 2016) from different hydrocarbon precursors. In this work, we studied SOA formed
163 from toluene photooxidation, limonene ozonolysis and α -pinene ozonolysis, 3 of the most
164 commonly studied SOA systems (Ng et al., 2007; Hildebrandt et al., 2009; Hartz et al.,
165 2005; Varutbangkul et al., 2006). Toluene (analytical standard, Sigma Aldrich) was injected
166 continuously into zero air flow by a syringe (1000 mL, Hamilton) installed on a syringe pump
167 (KDS Legato100) to achieve an initial concentration of 0.5 ppm. Limonene (Sigma-Aldrich,
168 97 %) and α -pinene (Sigma-Aldrich, 98 %) were pre-dissolved in cyclohexane (Sigma-Aldrich,
169 99.5 %) with a volumetric ratio of 1: 1500 and 1: 500 to ensure that OH formed from limonene
170 or α -pinene ozonolysis is scavenged by cyclohexane, estimated based on the rate constants
171 (Atkinson and Arey, 2003). The initial steady-state concentrations of limonene and α -pinene
172 were controlled to be around 2 ppm and 1 ppm entering the flow tube. O_3 , used as the oxidant
173 (for limonene and α -pinene) or the OH precursor (for toluene), was generated by passing 0.5 L
174 min^{-1} pure oxygen (99.6 %, Linde, Mississauga, Canada) through an O_3 generator (no.
175 97006601, UVP, Cambridge, UK). Humidified air was produced by bubbling zero air through a
176 custom-made humidifier at a flow rate of 1 L min^{-1} . The photolysis of O_3 produces $\text{O}(^1\text{D})$,
177 which reacts with water vapour to produce $\cdot\text{OH}$ with illumination from the 254 nm UV lamps
178 (UVP, Cambridge, UK) to initiate the photooxidation of toluene. The average residence time
179 inside the flow tube was controlled to be around 5 minutes. A gas chromatography–flame
180 ionization detector (GC-FID, model 8610C, SRI Instruments Inc., LV, USA) equipped with a

181 Tenax® TA trap was used to monitor the concentration of hydrocarbon precursors at the
182 inlet/outlet of the flow reactor. In all cases, the O₃ concentration was maintained to be at least 10
183 times higher than that of the hydrocarbon. Temperature and relative humidity were monitored by
184 an Omega HX94C RH/T transmitter. Particle size distribution and volume concentration were
185 monitored using a custom-built scanning mobility particle sizer (SMPS), which is a combination
186 of a differential mobility analyzer column (DMA, model 3081, TSI, Shoreview, MN, USA) with
187 flow controls and a condensation particle counter (CPC, model 3772, TSI, Shoreview, MN,
188 USA).

189

190 **2.2 Quantification of γ_{SO_2}**

191 Prior to each experiment, the chamber was flushed by purified air overnight with a flow rate of
192 25 L min⁻¹ until particle number concentration was less than 5 cm⁻³ and SO₂ was less than 1 ppb.
193 To adjust RH, the chamber was humidified by passing purified air through a custom-built
194 humidifier filled with ultra-pure water. For experiments with atomized ammonium sulfate or
195 malonic acid, SO₂ was injected into the chamber prior to the introduction of particles. For
196 experiments studying γ_{SO_2} onto SOA, aerosol generated from the flow tube was injected into the
197 Teflon chamber continuously after passing through an O₃ denuder (Ozone Solutions, Iowa, USA)
198 to achieve specific aerosol concentration inside the chamber prior to SO₂ addition. SO₂ mixing
199 ratio in the chamber during each experiment was continuously monitored using an SO₂ analyzer
200 (Model 43i, Thermo Scientific). The initial mixing ratio of SO₂ in each experiment was
201 controlled to be around 200 ppb. Aerosol size distribution was monitored by SMPS. The reactive
202 uptake coefficient of SO₂ was calculated by integrating the following equation:

$$203 \quad -\frac{d[SO_2]}{dt} = \frac{1}{4}\gamma_{SO_2}A\bar{c}[SO_2] \quad (1)$$

204

205 Where $[\text{SO}_2]$ is the SO_2 mixing ratio (ppb) monitored by the SO_2 analyzer; A is the average
206 surface area concentration ($\mu\text{m}^2 \text{cm}^{-3}$) derived from the particle size distribution measured by
207 SMPS; \bar{c} represents the mean molecular velocity (cm s^{-1}) of SO_2 . $d[\text{SO}_2]/dt$ is solved over the
208 initial SO_2 decay, such that the peroxide concentration in the aerosol liquid phase is assumed to
209 be constant and pseudo-first order kinetics can be applied (Abbatt et al., 2012; Thornton et al.,
210 2003). A summary of all the measured γ_{SO_2} can be found in Table S1. Typical evolution of
211 monitored species can be seen in Fig.1. Control experiments were performed in order to rule out
212 other potential factors (e.g. SO_2 loss in the in-line filter in front of the SO_2 analyzer, interferences
213 inside the SO_2 analyzer, chamber wall losses, SO_2 uptake onto wet ammonium sulfate, gas-phase
214 reaction of SO_2 with peroxide vapour) that may contribute to the SO_2 decay observed during the
215 γ_{SO_2} measurement inside the chamber (Fig. S3-S6). Measurement uncertainty and precision of
216 γ_{SO_2} in this study can be found in Table S1. Also, we observed there was SO_2 repartitioning from
217 the humid chamber wall in the presence of organic peroxide under high RH (Fig. S6b, RH 74%).
218 The observed SO_2 repartitioning rate was then applied to correct the γ_{SO_2} measured under high
219 RH conditions (above 70%, Expt.14), and this correction amounts to a 40% increase in
220 calculated γ_{SO_2} .

221

222 2.3 Offline peroxide quantification

223 Aerosol was collected onto 47 mm PTFE (polytetrafluoroethylene) filters with 0.2 μm pore size
224 (Whatman®, GE Healthcare) from the chamber by a diaphragm pump (KNF Neuberger Inc., USA)
225 for offline chemical analysis. The total particulate peroxide content (H_2O_2 , ROOH and ROOR) in
226 these samples prior to SO_2 uptake was quantified using the iodometric–spectrophotometric assay
227 (Docherty et al., 2005). I_2 produced from the reaction between I^- and peroxides can further quickly

Formatted: Line spacing: Double

Formatted: Subscript

Formatted: Subscript

228 combine with the excess amount of I^- to form I_3^- , which has brown color and absorbs UV-vis at
 229 470nm. The SOA extraction was then aliquoted into a 96-well UV plate (Greiner Bio-One,
 230 Kremsmünster, AT) with $160 \mu\text{L well}^{-1}$. $20 \mu\text{L}$ of formic acid ($\geq 95\%$, Sigma-Aldrich) was added
 231 into each well, following by $20 \mu\text{L}$ potassium iodide (BioUltra, $\geq 99.5\%$, Sigma-Aldrich) solution
 232 (dissolved in DI water). The plate was then covered by an adhesive plate sealer (EdgeBio,
 233 Gaithersburg, USA) immediately in order to avoid reagent evaporation and O_2 oxidation. After
 234 incubation for an hour in the dark, the UV-vis absorption at 470nm was measured using a UV-vis
 235 spectrophotometer (Spectramax 190, Molecular Devices Corporation, Sunnyvale, CA) and then
 236 converted to peroxide concentration using the calibration curve made by tert-butyl hydroperoxide

237 (70 wt. % in H_2O , Sigma-Aldrich) with a series of concentrations (0-10mM). An average
 238 molecular mass for seed particles (SOA + ammonium sulfate) was assumed based on the chemical
 239 composition in order to calculate the molar fraction of total peroxides using the following equation:

$$\text{Molar fraction of peroxide} = \frac{N_{\text{peroxide}}}{N_{\text{aerosol}}} = N_{\text{peroxide}} \frac{M_{(NH_4)_2SO_4} f_{(NH_4)_2SO_4} + M_{\text{peroxide}} f_{\text{peroxide}}}{m_{\text{aerosol}}}$$

243 where m_{aerosol} is the weighed aerosol mass on the filter; $M_{(NH_4)_2SO_4}$ and M_{peroxide} are the
 244 molecular mass of ammonium sulfate and peroxide, respectively; $f_{(NH_4)_2SO_4}$ and f_{peroxide} are the
 245 initial molar fraction of ammonium sulfate and peroxide; N_{peroxide} and N_{aerosol} are the
 246 measured peroxide molar and calculated aerosol molar, respectively. ~~The average molecular~~
 247 ~~mass for aerosol was assumed based on the chemical composition in order to calculate the molar~~
 248 ~~fraction of total peroxides.~~ More details about the iodometric-spectrophotometric procedures
 249 were described in previous work (Wang et al., 2018).

251 3 Results and discussion

Formatted: Font color: Text 1

Formatted

Formatted

Formatted

Formatted

Formatted

Formatted

Formatted

Formatted

Formatted

Formatted: English (Canada)

252 3.1 SO₂ uptake and RH

253 A positive relationship between γ_{SO_2} and RH (between 25 and 71%) was observed for all types of
254 organic peroxides studied (Fig. 2). The positive dependence of the reactive uptake coefficient of
255 water-soluble gaseous species on RH has also been observed in other studies (Thornton et al.,
256 2003;Griffiths et al., 2009;Zhao et al., 2017;Zhang et al., 2019). Recently, the uptake behavior of
257 SO₂ onto soot, mineral dust and SOA were also shown to positively depend on RH (Zhang et al.,
258 2019;Zhao et al., 2017;Yao et al., 2019).

259 It is also noteworthy that an exponential dependence of SO₂ reactive uptake coefficient on RH
260 was observed in our study. γ_{SO_2} increases with increased relative humidity, which could even be
261 more significant under high RH regime. This is consistent with previous laboratory studies that
262 measured the reactive uptake coefficient of SO₂ onto aerosol to be exponentially dependent on
263 RH (Zhang et al., 2019;Yao et al., 2019). Additionally, multiple field campaigns have observed
264 significant correlation between particulate sulfate formation and ambient RH (Song et al.,
265 2019;Sun et al., 2013;Huang et al., 2020). Sun et al. (2013) observed faster sulfate formation rate
266 under humid conditions, proposing a significant impact of aerosol liquid water on sulfate
267 production during wintertime in Beijing. Zheng et al. (2015) reported a notably higher SOR
268 (molar ratio of sulfate to the sum of sulfate and SO₂) during wet period (RH>50%), indicating
269 the importance of heterogeneous reactions to the secondary sulfur transformation with abundant
270 aerosol water content under humid conditions. In a recent study by Song et al. (2019), the rapid
271 sulfate formation rate observed under high RH conditions was found to be significantly higher
272 than atmospheric modeling results implemented with homogeneous SO₂ oxidation pathways,
273 which was later attributed to heterogeneous sulfate formation mechanisms. Multiple mechanisms
274 can potentially explain this observed γ_{SO_2} -RH dependence. An enhanced relative humidity would

275 result in a nonlinear increase of aerosol water content, which can lead to more SO₂ dissolved in
276 the aerosol aqueous phase (Seinfeld and Pandis, 2012). It should be noted that while the relative
277 humidity is varied systematically in these experiments, the relationship is more complex since
278 RH also affects other aerosol properties which can affect the uptake kinetics in turn. For
279 example, a higher aerosol liquid water content could dilute protons and thus lower the aerosol
280 acidity. In a study by Laskin et al. (2003), an enhanced uptake of SO₂ onto sea-salt particles was
281 observed with an increased aerosol alkalinity at high pH range.

282 283 **3.2 Dependence of SO₂ uptake on peroxide content and type**

284 As expected, the measured uptake rate of SO₂ is dependent on the particulate peroxide content in
285 the current study. Fig. 3 shows that γ_{SO_2} is linearly proportional to the amount of particulate
286 peroxide for aerosol with similar volume-to-surface ratios and containing the same type of
287 organic peroxides. This positive relationship between γ_{SO_2} and condensed phase peroxide content
288 has also been inferred from experiments of SO₂ uptake onto α -pinene SOA (Yao et al., 2019),
289 where the peroxide content in α -pinene SOA was varied indirectly by introducing NO and
290 adjusting the branching ratio of the peroxide-yielding RO₂+HO₂/RO₂ pathway.

291 In addition to the amount of peroxide injected, the particulate fraction of organic peroxide
292 available for heterogeneous reaction is also influenced by gas-particle partitioning. As indicated
293 in Fig. 2, the reactive uptake coefficients of different organic peroxides vary amongst each other
294 by about an order of magnitude in the range of RH studied, despite the same amounts of peroxide
295 relative to ammonium sulfate initially in the atomizing solution. Based on our previous work
296 (Wang et al., 2019), the aqueous-phase rate constants for these organic peroxides with dissolved
297 S(IV) only vary by a factor of 2-3 and therefore cannot fully explain the observed difference in

298 uptake rates. Since vapour pressure vary considerably among the different peroxides in the
299 present study, gas-particle partitioning is likely to influence the amount of peroxide in the
300 particle phase that react with dissolved SO₂. The relative particulate peroxide content on filters
301 of the three peroxides collected from chamber experiments under RH 50% without SO₂ uptake
302 were measured by the offline KI method (Fig. S7). Although the initial ratio of organic peroxide
303 to ammonium sulfate in the atomizing solution was nominally the same, we measured the highest
304 amount of particulate peroxide with 2-butanone peroxide (16.7%), followed by cumene
305 hydroperoxide (12.7%) and then tert-butyl hydroperoxide (3.8%) using the offline iodometric
306 method. This trend in particulate peroxide content is consistent with the vapour pressures
307 calculated using the SIMPOL group contribution method (Pankow et al., 2008), with 2-butanone
308 peroxide being the least volatile, and tert-butyl hydroperoxide being the most volatile. Also, the
309 order of particle-phase peroxide content is consistent with the order of γ_{SO_2} observed, as shown in
310 Fig. 2. A simple visualization of these relationships between different peroxide characteristics
311 (number of peroxide groups, vapour pressure and aqueous-phase rate constants) and measured
312 γ_{SO_2} (at RH = 50%) is illustrated in Fig. S7, which indicates higher γ_{SO_2} can be expected for
313 ~~multifunctional~~ organic peroxides with multiple O-O groups, ~~with~~ lower vapour pressures and
314 higher aqueous phase reactivities. It should be noted that the order of magnitude difference in
315 experimentally measured γ_{SO_2} among various organic peroxides (Fig.2) is still not fully explained
316 when both volatility and reaction kinetics are taken into account (Fig.S7), suggesting that the
317 reactive uptake may be influenced by other factors. In summary, for our current experiments
318 where we nominally maintained total injected amount of organic peroxide constant, measured
319 γ_{SO_2} depends both on reactivity and gas-particle partitioning of the organic peroxides.
320

321 **3.3 SO₂ uptake and aqueous phase kinetics**

322 Since the aqueous phase reaction rate constants between S(IV) and these model organic
323 peroxides have been measured previously (Wang et al., 2019), we can test our understanding of
324 the measured γ_{SO_2} using a simple model. By assuming the amount of SO₂ dissolved in the aerosol
325 is in equilibrium with the gas phase, the overall γ_{SO_2} can be expressed using the simplified
326 resistor model (Hanson et al., 1994):

327

$$\frac{1}{\gamma} = \frac{1}{\alpha} + \frac{\bar{c}}{4HRT\sqrt{k^l D_l}} \frac{1}{\left[\coth(q) - \frac{1}{q}\right]} \quad (2)$$

328

329 where α is the mass accommodation coefficient, \bar{c} is the mean molecular speed of SO₂ (cm s⁻¹),
330 H is the effective Henry's law constant that includes both the dissolution of SO₂ and the
331 dissociation of H₂SO₃ (M atm⁻¹), R is the ideal gas constant (atm L mol⁻¹ K⁻¹), T is the
332 temperature (K), and the parameter q is used to describe the competition between the reaction
333 and diffusion of the dissolved gaseous species within a particle, which is further calculated as:

334

$$q = r \sqrt{\frac{k^l}{D_l}} \quad (3)$$

335 where r is the radius (cm) of a given particle, D_l is the aqueous-phase diffusion coefficient (cm²
336 s⁻¹), k^l is the first order rate constant (s⁻¹) for the reaction. For experiments in the current study,
337 the calculated q values were consistently found to be far less than 1, which indicates a volume-
338 limited reaction regime. Combining with the assumption of a relatively fast mass
339 accommodation process compared with the bulk phase reaction, equation (2) can be further
340 simplified as to describes reactive uptake in the volume-limited regime:

341

$$\gamma = \frac{4HRT[\text{peroxide}]k^l V}{\bar{c} S} \quad (4)$$

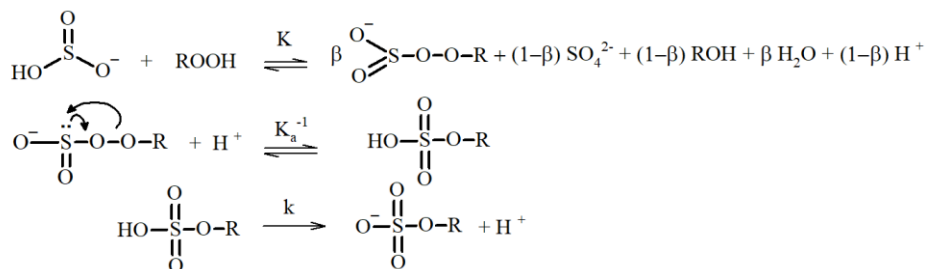
342 Here, we assume all the peroxides remain in the condensed phase upon atomizing and reaction
343 inside the chamber for the upper-bound prediction of γ_{SO_2} . [peroxide] represents the particle phase

344 concentration of total organic peroxide (M) based on the initial ratio between organic peroxide and
345 ammonium sulfate in the atomizing solution, and the aerosol water content output by E-AIM III
346 (Clegg et al., 1998), k^{II} is the second order reaction rate constant ($\text{M}^{-1} \text{s}^{-1}$), which we have
347 measured in the bulk phase at dilute concentrations previously (Wang et al., 2019), V/S is the ratio
348 between particle volume concentration ($\mu\text{m}^3 \text{cm}^{-3}$) and particle surface area concentration (μm^2
349 cm^{-3}) derived from SMPS measurements. As a result, the observed reactive uptake coefficient of
350 SO_2 can be compared to that predicted from the bulk phase reaction rate constant, and the results
351 are shown in Fig. 4 and Fig. S8. Overall, we noticed that this model captures the dependence of
352 γ_{SO_2} on peroxide content, but the modeled results were found to be generally 15-50 times lower
353 than the experimentally measured values (Fig. S8). The current γ_{SO_2} predictions are likely upper-
354 bound estimates since all the peroxides were assumed to stay in the condensed phase without
355 partitioning. As a result, this observed 15-50 times of discrepancy could even be larger if the
356 particulate peroxide content during the chamber experiments were lower due to partitioning.

357 It should be noted that the calculated γ_{SO_2} was based on reaction kinetics measured in dilute
358 solutions while the experimental γ_{SO_2} were measured directly from suspended particles. This large
359 difference in kinetics between those in aerosol and in dilute bulk solution suggests that this
360 multiphase interaction is strongly favored in the highly concentrated aerosol environment. One of
361 the potential explanations for this discrepancy could be liquid-liquid phase separation (LLPS) in
362 aerosol between organic peroxide and ammonium sulfate (Ciobanu et al., 2009; O'Brien et al.,
363 2015) such that SO_2 can directly interact with the acidic organic phase, where the concentration of
364 peroxides can be higher and the kinetics can be different from what we have measured in dilute
365 solution (Wang et al., 2019). However, LLPS is generally governed by the chemical composition
366 of the hydrophobic phase (Freedman, 2017). A higher level of oxygenation in organic aerosol is

367 related with higher hydrophilicity, which would favor a homogeneous particle instead of phase
 368 separation. Previous studies showed that LLPS did not occur for organic coating with O:C above
 369 0.8 (You et al., 2013; You et al., 2014). The LLPS phenomenon in simple organic-inorganic
 370 mixtures can also be affected by the functional groups. The maximum O:C for LLPS could be 0.71
 371 for organics with multiple carboxylic and hydroxyl groups but low aromatic content (Song et al.,
 372 2012) while the 2-butanone peroxide we used for both γ_{SO_2} measurement and prediction in the
 373 present study has multiple peroxide groups with an O:C value of 0.75. Particle size could also have
 374 impacts on phase separation (Cheng et al., 2015). Particle diameters in the current study are mainly
 375 under 200 nm while a previous study showed particles smaller than this size are less likely to
 376 experience LLPS (Veghte et al., 2013). We therefore believe that LLPS is not likely to be
 377 responsible for the enhanced uptake rate observed under these experimental conditions.

378 Another explanation is the high solute strength in the concentrated aerosol phase. Although the
 379 aerosol water content for ammonium sulfate aerosol was found to be higher than that of malonic
 380 acid aerosol under RH 50%. As indicated in Fig. 4 and Fig. S8, the difference between the
 381 measured and predicted γ_{SO_2} is larger for ammonium sulfate aerosol than for malonic acid.
 382 Meanwhile, the calculated ionic strength in aerosol liquid phase under RH 50% for ammonium
 383 sulfate (40 mol kg⁻¹) is significantly larger than that of malonic acid (0.45 mol kg⁻¹). It has been
 384 previously reported that the reaction rate between sulfite and hydrogen peroxide in aqueous phase
 385 increases with ionic strength (Maaß et al., 1999). Based on the reaction mechanisms proposed for



Formatted: Font: 12 pt

Formatted: Font: 6 pt

Formatted: Font: 12 pt

Formatted: Font: 12 pt

386 dissolved SO₂ and hydrogen peroxide (Halperin and Taube, 1952), we speculate the reaction
387 between aqueous phase S(IV) and organic peroxides to follow a similar mechanism:

388
389 where the overall rate constant is equal to $k \frac{K}{K_a}$, assuming fast equilibrium steps for reactions 5 and
390 6. Dissociated solutes are surrounded by an extended solvation shell which could affect the
391 reaction rates (Herrmann, 2003). Fewer available free water molecules would therefore shift the
392 equilibrium to the right in equation (5). Additionally, higher ionic strength also corresponds to an
393 increased concentration of electrolytes in the aqueous phase, which could hinder the dissociation
394 of the peroxy monosulfurous acid and shift the equilibrium in equation (6) to the right. In recent
395 work by Liu et al. (2020), the rate of S(IV) oxidation by H₂O₂ can be enhanced by up to a factor
396 of 50 in aerosol aqueous phase compared to that of dilute solution. The highest ionic strength at
397 which such enhancement was measured for the H₂O₂ oxidation pathway was 15 mol kg⁻¹ (Liu et
398 al., 2020).

399 Whereas the above analysis is based on the assumption that all the chemistry occurs in the bulk
400 component of the particle, it is also possible that some component of the reaction occurs at the gas-
401 particle interface and the overall kinetics can be affected by interfacial characteristics. For example,
402 an enhanced ionic strength in the aerosol phase can also impact the interfacial reaction mechanisms.
403 Previous study has shown evidence that interfacial chemistry is important for SO₂ oxidation in the
404 aerosol phase (Laskin et al., 2003). With higher ionic strength, anions partitioning to the air-liquid
405 interface can promote the overall reaction kinetics via proton transfer and thus accelerate the
406 interfacial chemistry (Knipping et al., 2000; Mishra et al., 2012; Mekic et al., 2018; Mekic et al.,

407 2020; Wei et al., 2018; Ruiz-Lopez et al., 2020). In addition to the catalytic effects of protons
408 indicated in Eqn.5-7, Hung et al. (2015, 2018) observed significant SO₃⁻ signal at the acidic

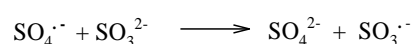
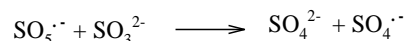
Formatted: Not Highlight

Formatted: Subscript

Formatted: Font: Bold, Superscript

Formatted: Superscript

409 microdroplet surface, which can promote sulfate formation via radical propagation chain initiated
410 by surrounding radicals and molecular oxygen (Eqn. 8-11):



411
412 where the hydroxy radical can potentially be produced from decomposition of the labile organic
413 peroxide in our system (Tong et al., 2016). However, we cannot distinguish whether the interfacial
414 protons promote sulfate formation by catalyze the peroxide S(IV) oxidation pathway or the sulfur
415 radical pathway at the current stage. In the recent study by Wei et al. (2018), a pH gradient was
416 observed for phosphate-buffered aerosol droplets with the proton accumulated at the interface.
417 Base on the pH-dependent aqueous phase kinetics measured in our previous work (Wang et al.,
418 2019), such interfacial proton accumulation could potentially explain the enhanced kinetics we
419 observed for aerosol in the current study. However, the chemical compositions are quite different.
420 While phosphate-buffered particles were studied in Wei et al. (2018), acidic ammonium sulfate
421 aerosol was used in our study. Also, the particle size in Wei et al. (2018) is significantly larger (20
422 um) than what was studied in the current study (200 nm). However, it should be noted that
423 there is no direct evidence from the current study showing the direct relationship between the
424 interfacial properties and γ_{SO_2} , and future studies are warranted.

425 Therefore, while more studies are needed to clearly delineate the roles of ionic strength, interfacial
426 activity, bulk reactivity, and particle phase state quantitatively, the enhancement of SO_2 oxidation

Formatted: Font: 12 pt

Formatted: Font: 12 pt

Formatted: Font: 12 pt

Formatted: Font: 12 pt

Formatted: Not Highlight

427 kinetics by highly concentrated aerosol particles compared to dilute aqueous solutions are
428 concluded to be large (factor of 15-50) for the experimental conditions in the current study.

429

430 **3.4 SO₂ uptake and aerosol pH**

431 As indicated by the proposed reaction mechanisms (Eqn. 5-7), protons are important reaction
432 intermediates for this SO₂ oxidation pathway. Previously, the aqueous phase reaction rate
433 constants between organic peroxides and dissolved SO₂ were measured to be pH dependent
434 (Wang et al., 2019). Moreover, the dissolution equilibrium of SO₂ into aqueous phase is also pH
435 sensitive (Seinfeld and Pandis, 2012). Besides, many studies have shown that the uptake kinetics
436 for gaseous species can be affected by the condensed phase pH (Shi et al., 1999; Gaston et al.,
437 2014; Drozd et al., 2013; Jang and Kamens, 2001; Liu et al., 2015). Reactive uptake of ammonia
438 was observed to depend on condensed phase acidity (Shi et al., 1999). Heterogeneous
439 condensation of isoprene-derived epoxydiol onto seed aerosol was found to increase with proton
440 concentration (Gaston et al., 2014). In the current study, the potential impact from particle phase
441 pH on γ_{SO_2} was explored by adding HCl into the atomizing solution. To estimate the particle
442 phase pH, two different methods associated with two different assumptions were used. In the
443 first scenario, the aerosol pH in each experiment was estimated using the E-AIM III model
444 (Clegg et al., 1998) based on the initial molar ratios of inorganic species (H^+ , NH_4^+ , SO_4^{2-} , Cl^-) in
445 the atomizing solution and measured RH (around 50%). In the second scenario, the additional
446 sulfate formed from reactive uptake of SO₂ was taken into consideration. The partitioning of HCl
447 was allowed in the model simulation for both scenarios. The formation of sulfate would enhance
448 the proton concentration in the aerosol liquid phase thus lower the aerosol pH. The average pH
449 during the SO₂ uptake process is likely in between these two extremes.

450 Fig. 5 shows the measured reactive uptake coefficients of SO₂ as a function of the calculated pH.
451 The reactive uptake coefficient was found to weakly increase with ~~increasing proton~~
452 ~~concentrations~~decreasing pH (decreasing pH), which is consistent with acid-catalyzed reactions
453 between peroxides and dissolved SO₂ as measured in the bulk phase (Lind et al., 1987; Wang et
454 al., 2019). γ_{SO_2} was also predicted for the same range of pH based on Eqn. 4 and the pH-
455 dependent bulk-phase reaction rate constants measured previously (Wang et al., 2019). Indicated
456 by Fig. 5, the measured γ_{SO_2} again exceeds the predicted γ_{SO_2} by about a factor of 50, which is
457 consistent with what we reported earlier and is likely due to the effects of aerosol ionic strength.
458 Unlike the observed γ_{SO_2} , however, the predicted γ_{SO_2} does not exhibit a monotonic trend. γ_{SO_2} is
459 expected to decrease with decreasing pH at high pH (>2) as the effective Henry's law constant of
460 SO₂ decreases with higher acidity (Seinfeld and Pandis, 2012). γ_{SO_2} is not expected to increase
461 with decreasing pH until pH is below 2 where the acidity enhancement in reaction rate constant
462 exceeds the decrease in SO₂ solubility. As illustrated earlier, extrapolating dilute aqueous-phase
463 kinetics to the highly concentrated aerosol requires considering effects from high solute strength.
464 Solute strength may change the pH dependence of γ_{SO_2} in two ways. First, the solubility of SO₂
465 may decrease and become less dependent on pH as ionic strength increases (Rodríguez-Sevilla et
466 al., 2002). A former study (Leng et al., 2015) has shown that the effective Henry's law of
467 triethylamine decreases with increased ionic strength. Another potential explanation is that the
468 aqueous phase reaction rate constant can be more pH-dependent at high ionic strengths than what
469 we measured previously in dilute solutions. In either case, the inflection of the predicted γ_{SO_2}
470 would change and γ_{SO_2} could become more negatively dependent on pH ($d[\gamma_{\text{SO}_2}]/d[\text{pH}]$ becomes
471 less positive in the high pH range and/or more negative in the low pH range), which would
472 match more closely with the observed dependence. It should also be noted that there are

473 substantial uncertainties in estimating pH values, originating from the partitioning of organics,
474 organic-inorganic phase separations, mixing state of specific ions, uncertain activity coefficients
475 and the propagation of RH uncertainties (Clegg et al., 2008; Fountoukis et al., 2009; Guo et al.,
476 2016). ~~since~~ Also, the reactive uptake is a dynamic process and will influence aerosol pH in turn
477 upon sulfate formation. In summary, while the magnitude of predicted γ_{SO_2} is consistent with our
478 expected values (after accounting for the enhancement by high aerosol solute strength), we
479 cannot fully explain the dependence of γ_{SO_2} on aerosol pH at the current stage. Future studies
480 should investigate how the effective Henry's law of SO_2 and pH dependence of reaction rate
481 constants vary in aerosol liquid phase with high solute strength in order to have a more
482 comprehensive understanding of the relationship between γ_{SO_2} and aerosol pH.

483 **3.4 SO_2 uptake onto SOA**

484 γ_{SO_2} was measured for a few model SOA systems, as organic peroxides are abundant in SOA
485 (Surratt et al., 2006; Kautzman et al., 2009; Krapf et al., 2016; Bonn et al., 2004). Here we studied
486 SOA formed from monoterpene ozonolysis and toluene photooxidation. It should be noted that
487 for the γ_{SO_2} measurements of toluene SOA, a strong hydrocarbon interference was observed with
488 the SO_2 analyzer, likely stemming from the high concentrations of gas-phase aromatic
489 compounds. A rough estimate of the uptake rate for toluene SOA from aerosol mass
490 spectrometer sulfate measurements is provided in the SI (Section 1). The reactive uptake
491 coefficient of SO_2 onto Saharan mineral dust was reported on the order of 10^{-5} (Adams et al.,
492 2005). γ_{SO_2} onto dust with the coexistence of NO_2 and NH_3 under various RH conditions were
493 measured to be 10^{-7} to 10^{-5} (Zhang et al., 2019). For a variety of metal oxides, SO_2 reactive
494 uptake coefficients were quantified to be between 10^{-6} and 10^{-4} (Usher et al., 2002; Fu et al.,
495 2007; Shang et al., 2010). More recently, γ_{SO_2} studied for heterogeneous sulfate formation by

496 photolysis of particulate nitrate were reported in the range of 10^{-6} to 10^{-5} (Gen et al., 2019). As
497 shown in Fig. 6, γ_{SO_2} for all SOA systems were measured to be on the order of 10^{-4} . Similar γ_{SO_2}
498 values on the order of 10^{-4} were measured for α -pinene SOA by Yao et al. (2019), and 10^{-5} for
499 limonene SOA estimated from the chamber study by Ye et al. (2018). The reaction products
500 from this SOA and SO_2 interaction will be reported in a separate study.

501

502 **4. Atmospheric Implications**

503 Oxidation of atmospheric hydrocarbons produces reactive intermediates that can potentially
504 interact with SO_2 and form particulate sulfate, contributing to PM formation and growth (Berndt
505 et al., 2015;Mauldin et al., 2012;Yao et al., 2019). Organic peroxides generated from both
506 biogenic and anthropogenic hydrocarbon emissions are abundant in submicron aerosol. Given
507 that they are highly reactive with relatively short lifetimes (Bonn et al., 2004;Krapf et al.,
508 2016;Qiu et al., 2020), these species could serve as important condensed phase oxidants for gas
509 phase SO_2 . Combining laboratory measurements and model predictions, the current study
510 investigated heterogeneous reactions between SO_2 and particulate organic peroxide. The
511 measured γ_{SO_2} for organic peroxide containing aerosol ranges from 10^{-5} to 10^{-2} in this study.
512 Based on the modeling work by Wang et al. (2014), adding an SO_2 uptake pathway to GEOS-
513 Chem with a reactive uptake coefficient of 10^{-4} could improve the surface sulfate prediction by
514 more than 50% during a severe haze episode over North China (RH 50%), suggesting the
515 potential importance of this multiphase reaction pathway, especially when SOA is the dominant
516 component in particulate matter.
517 The dependence of the heterogeneous kinetics on RH, aerosol pH, peroxide type, and peroxide
518 content were also evaluated. The experimentally measured γ_{SO_2} was found to be consistently

519 higher than that predicted from reaction kinetics with organic peroxides in the dilute aqueous
520 phase. This discrepancy can be potentially explained by the effects of high ionic strength
521 presented in the aerosol, suggesting that the impact from highly concentrated solutes needs to be
522 taken into consideration when applying aqueous phase kinetics to aerosol multiphase chemistry,
523 especially for particles containing strong electrolytes. We also observed that the kinetics of this
524 multiphase reaction exhibit a weak dependence on pH. Increasing the condensed-phase acidity
525 ~~may enhances~~ the heterogeneous rate constant at low pH ~~range~~, and while this pH dependence is
526 consistent with that of the aqueous phase reaction rate constant measured previously, it is not
527 consistent with the decrease of effective Henry's law constant of SO₂ along with enhanced
528 acidity. Also, it is likely that within the uncertainties, there may not be an observable γ_{SO_2} -pH
529 trend. Currently, we are not able to fully explain the pH dependence, ~~likely due to the~~
530 ~~uncertainties from high ionic strength~~, and further studies are warranted. Particle phase peroxide
531 content was observed to be linearly correlated with γ_{SO_2} . Moreover, γ_{SO_2} measured for 2-butanone
532 peroxide was found to be orders of magnitude higher than that of cumene hydroperoxide and
533 tert-butyl hydroperoxide. The difference in γ_{SO_2} among various types of organic peroxides can be
534 partially explained by their condensed-phase reactivity and gas-particle partitioning.
535 In general, we found the observed γ_{SO_2} in this study can be summarized using the following
536 semiempirical multilinear relationship:

$$537 \quad \log \gamma = -1.7 + 0.0024 \times k'' + 0.46 \times PAS + 0.024 \times RH - 1.9 \times Vp \quad (8)$$

538 where γ is the reactive uptake coefficient, k'' is the aqueous phase S(IV) oxidation rate constant
539 ($\text{M}^{-1} \text{s}^{-1}$), PAS is the molar ratio between particulate peroxide and ammonium sulfate in the
540 atomizing solution, which is a proxy for the amount of peroxide in both gas and particle phases
541 applied in the current study, RH is the relative humidity (%), Vp is the vapour pressure (kPa) of

542 the peroxide. Fig. 7 illustrates the degree to which this semi-empirical expression describes the
543 experimental data for ammonium sulfate aerosol mixed with the three types of organic peroxides.
544 Residual evaluations of this multilinear regression can be found Fig. S9. We caution that this
545 equation is not directly applicable to atmospheric models in its current form, especially since the
546 particle phase peroxide content (PAS) value we applied as input is a calculated value, rather than
547 a measurement. However, it illustrates the internal consistency of our experimental results across
548 a range of RH, peroxide content, and aqueous phase reactivities, which are the key variables for
549 uptake rates. Better understanding of ionic strengths and pH in aerosol, either through modeling
550 or direct measurements of these variables, is needed to establish the coefficient dependence.
551 Future studies should be focused on exploring γ_{SO_2} and the reaction products for various types of
552 SOA as well as ambient particles under atmospherically relevant conditions, evaluating the
553 underlying impacts from photochemical condition, chemical composition, particle morphology,
554 ionic strength and interfacial properties on this multiphase physicochemical process. Overall,
555 γ_{SO_2} presented in our study and its relationship with ambient RH, aerosol pH, ionic strength,
556 particulate peroxide content and type could provide a framework for the implementation of this
557 heterogeneous mechanism in atmospheric models to have a better understanding of ambient
558 sulfate formation and particle growth.

559

560

561

562

563

564

565 *Author contributions*

566 A.W.H. C. and S.W. designed the study. S.W., T. L., and J. J. performed the experiments. S.W.,
567 A.W.H. C., T. L., and J. J. analyzed data. S.W. and A.W.H. C. wrote the manuscript with the
568 input from all co-authors.

569

570 *Data availability*

571 All data presented in this study are available in the supplemental material and have been
572 deposited in figshare.

573

574 *Associated content*

575 Supporting Information.

576

577 *Competing interests*

578 The authors declare no competing financial interest.

579

580 *Acknowledgements*

581 This work was supported by Natural Sciences and Engineering Research Council Discovery Grant.

582 The authors would like to thank Dr. Greg Evans, Dr. Yue Zhao and Dr. Christopher Lim for helpful
583 comments and discussions. Special thanks to SOCAAR for providing the SO₂ analyzer.

584

585

586

587

588

589 **Reference**

- 590 Abbatt, J. P. D., Lee, A. K. Y., and Thornton, J. A.: Quantifying trace gas uptake to tropospheric
591 aerosol: recent advances and remaining challenges, *Chem. Soc. Rev.*, 41, 6555–6581,
592 <https://doi.org/10.1039/c2cs35052a>, 2012.
- 593 Adams, J. W., Rodriguez, D., and Cox, R. A.: The uptake of SO₂ on Saharan dust: a flow tube
594 study, *Atmos. Chem. Phys.*, 5, 2643–2676, doi:10.5194/acp-5-2643-2005, 2005.
- 595 Andreae, M.O., Afchine, A., Albrecht, R., Holanda, B.A., Artaxo, P., Barbosa, H.M., Borrmann,
596 S., Cecchini, M.A., Costa, A., Dollner, M. and Fütterer, D.: Aerosol characteristics and particle
597 production in the upper troposphere over the Amazon Basin, *Atmos. Chem. Phys.*, 18, 921–961,
598 2018.
- 599 Atkinson, R., and Arey, J.: Atmospheric degradation of volatile organic compounds, *Chem.*
600 *Rev.*, 103, 4605-4638, 2003.
- 601 Berndt, T., Richters, S., Kaethner, R., Voigtländer, J., Stratmann, F., Sipilä, M., Kulmala, M.,
602 and Herrmann, H.: Gas-phase ozonolysis of cycloalkenes: Formation of highly oxidized RO₂
603 radicals and their reactions with NO, NO₂, SO₂, and other RO₂ radicals, *J. Phys. Chem. A*, 119,
604 10336-10348, 10.1021/acs.jpca.5b07295, 2015.
- 605 Bianchi, F., Kurtén, T., Riva, M., Mohr, C., Rissanen, M. P., Roldin, P., Berndt, T., Crouse, J.
606 D., Wennberg, P. O., Mentel, T. F., Wildt, J., Junninen, H., Jokinen, T., Kulmala, M., Worsnop,
607 D. R., Thornton, J. A., Donahue, N., Kjaergaard, H. G., and Ehn, M.: Highly oxygenated organic
608 molecules (HOM) from gas-phase autoxidation involving peroxy radicals: A key contributor to
609 atmospheric aerosol, *Chem. Rev.*, 119, 3472-3509, 10.1021/acs.chemrev.8b00395, 2019.
- 610 Bonn, B., von Kuhlmann, R., and Lawrence, M. G.: High contribution of biogenic
611 hydroperoxides to secondary organic aerosol formation, *Geophys. Res. Lett.*, 31, L10108,
612 <https://doi.org/10.1029/2003GL019172>, 2004.
- 613 Chen, Q., Farmer, D. K., Schneider, J., Zorn, S. R., Heald, C. L., Karl, T. G., Guenther, A.,
614 Allan, J. D., Robinson, N., Coe, H., Kimmel, J. R., Pauliquevis, T., Borrmann, S., Pöschl, U.,
615 Andreae, M. O., Artaxo, P., Jimenez, J. L., and Martin, S. T.: Mass spectral characterization of
616 submicron biogenic organic particles in the Amazon Basin, *Geophys. Res. Lett.*, 36, L20806,
617 <https://doi.org/10.1029/2009GL039880>, 2009.
- 618 Chen, T., Chu, B., Ge, Y., Zhang, S., Ma, Q., He, H., and Li, S.-M.: Enhancement of aqueous
619 sulfate formation by the coexistence of NO₂/NH₃ under high ionic strengths in aerosol water,
620 *Environ. Pollut.*, 252, 236-244, <https://doi.org/10.1016/j.envpol.2019.05.119>, 2019.
- 621 Cheng, Y., Su, H., Koop, T., Mikhailov, E., and Pöschl, U.: Size dependence of phase transitions
622 in aerosol nanoparticles, *Nat. Commun.*, 6, 5923, 10.1038/ncomms6923, 2015.
- 623 Cheng, Y. F., Zheng, G. J., Wei, C., Mu, Q., Zheng, B., Wang, Z. B., Gao, M., Zhang, Q., He, K.
624 B., Carmichael, G., Pöschl, U., and Su, H.: Reactive nitrogen chemistry in aerosol water as a
625 source of sulfate during haze events in China, *Sci. Adv.*, 2, e1601530, [https://doi.org/10.1126/](https://doi.org/10.1126/sciadv.1601530)
626 [sciadv.1601530](https://doi.org/10.1126/sciadv.1601530), 2016.

627 Ciobanu, V. G., Marcolli, C., Krieger, U. K., Weers, U., and Peter, T.: Liquid-liquid phase
628 separation in mixed organic/inorganic aerosol particles, *J. Phys. Chem. A*, 113, 10966–10978,
629 2009.

630 Clegg, S. L., Brimblecombe, P., and Wexler, A. S.: Thermodynamic model of the system
631 $\text{H}^+ - \text{NH}_4^+ - \text{Na}^+ - \text{SO}_4^{2-} - \text{NO}_3^- - \text{Cl}^- - \text{H}_2\text{O}$ at 298.15 K, *J. Phys. Chem. A*, 102, 2155–2171,
632 <https://doi.org/10.1021/jp973043j>, 1998.

633 [Clegg, S. L., Kleeman, M. J., Griffin, R. J., and Seinfeld, J. H.: Effects of uncertainties in the
634 thermodynamic properties of aerosol components in an air quality model – Part 1: Treatment of
635 inorganic electrolytes and organic compounds in the condensed phase, *Atmos. Chem. Phys.*, 8,
636 1057–1085, <http://www.atmos-chem-phys.net/8/1057/2008/>, 2008.](#)

637 Docherty, K. S., Wu, W., Lim, Y. B., and Ziemann, P. J.: Contributions of organic peroxides to
638 secondary aerosol formed from reactions of monoterpenes with O_3 , *Environ. Sci. Technol.*, 39,
639 4049–4059, 2005.

640 Dovrou, E., Rivera-Rios, J. C., Bates, K. H., and Keutsch, F. N.: Sulfate formation via cloud
641 processing from isoprene hydroxyl hydroperoxides (ISOPOOH), *Environ. Sci. Technol.*, 53,
642 12476–12484, [10.1021/acs.est.9b04645](https://doi.org/10.1021/acs.est.9b04645), 2019.

643 Drozd, G. T., Woo, J. L., and McNeill, V. F.: Self-limited uptake of α -pinene oxide to acidic
644 aerosol: the effects of liquid-liquid phase separation and implications for the formation of
645 secondary organic aerosol and organosulfates from epoxides, *Atmos. Chem. Phys.*, 13, 8255–
646 8263, doi:10.5194/acp-13-8255-2013, 2013.

647 Epstein, S. A., Blair, S. L., and Nizkorodov, S. A.: Direct photolysis of α -pinene ozonolysis
648 secondary organic aerosol: effect on particle mass and peroxide content, *Environ. Sci. Technol.*,
649 48, 11251–11258, 2014.

650 Fairlie, T. D., Jacob, D. J., Dibb, J. E., Alexander, B., Avery, M. A., van Donkelaar, A., and
651 Zhang, L.: Impact of mineral dust on nitrate, sulfate, and ozone in transpacific Asian pollution
652 plumes, *Atmos. Chem. Phys.*, 10, 3999–4012, doi:10.5194/acp-10-3999-2010, 2010.

653 [Fountoukis, C., Nenes, A., Sullivan, A., Weber, R., Van Reken, T., Fischer, M., Matas, E.,
654 Moya, M., Farmer, D., and Cohen, R. C.: Thermodynamic characterization of Mexico City
655 aerosol during MILAGRO 2006, *Atmos. Chem. Phys.*, 9, 2141–2156, \[http://www.atmos-chem-
phys.net/9/2141/2009/\]\(http://www.atmos-chem-
656 phys.net/9/2141/2009/\), 2009.](#)

657 Freedman, M. A.: Phase separation in organic aerosol, *Chem. Soc. Rev.*, 46, 7694–7705,
658 <https://doi.org/10.1039/C6CS00783J>, 2017.

659 Fu, H. B., Wang, X., Wu, H. B., Yin, Y., and Chen, J. M.: Heterogeneous uptake and oxidation
660 of SO_2 on iron oxides, *J. Phys. Chem. C*, 111, 6077–6085, 2007.

661 Gao, M., Carmichael, G. R., Wang, Y., Saide, P. E., Yu, M., Xin, J., Liu, Z., and Wang, Z.:
662 Modeling study of the 2010 regional haze event in the North China Plain, *Atmos. Chem. Phys.*,
663 16, 1673–1691, <https://doi.org/10.5194/acp-16-1673-2016>, 2016.

664 Gaston, C. J., Riedel, T. P., Zhang, Z., Gold, A., Surratt, J. D., and Thornton, J. A.: Reactive
665 uptake of an isoprene-derived epoxydiol to submicron aerosol particles, *Environ. Sci. Technol.*,
666 48, 11178–11186, [10.1021/es5034266](https://doi.org/10.1021/es5034266), 2014.

Formatted: Default Paragraph Font, Font: (Default) Calibri, 11 pt, Font color: Text 1, Do not check spelling or grammar

Formatted: Default Paragraph Font, Font: (Default) Calibri, 11 pt, Font color: Text 1, Do not check spelling or grammar

667 Gen, M., Zhang, R., Huang, D. D., Li, Y., and Chan, C. K.: Heterogeneous SO₂ oxidation in
668 sulfate formation by photolysis of particulate nitrate, *Environ. Sci. Tech. Let.*, 6, 86–91,
669 <https://doi.org/10.1021/acs.estlett.8b00681>, 2019.

670 Griffiths, P. T., Badger, C. L., Cox, R. A., Folkers, M., Henk, H. H., and Mentel, T. F.: Reactive
671 uptake of N₂O₅ by aerosols containing dicarboxylic acids. Effect of particle phase, composition,
672 and nitrate content, *J. Phys. Chem. A*, 113, 5082–5090, [10.1021/jp8096814](https://doi.org/10.1021/jp8096814), 2009.

673 Gunz, D. W. and Hoffmann, M. R.: Atmospheric chemistry of peroxides: A review, *Atmos.*
674 *Environ.*, 24A, 1601–1633, [https://doi.org/10.1016/0960-1686\(90\)90496-A](https://doi.org/10.1016/0960-1686(90)90496-A), 1990.

675 [Guo, H., Sullivan, A. P., Campuzano-Jost, P., Schroder, J. C., LopezHilfiker, F. D., Dibb, J. E.,](#)
676 [Jimenez, J. L., Thornton, J. A., Brown, S. S., Nenes, A., and Weber, R. J.: Fine particle pH](#)
677 [and the partitioning of nitric acid during winter in the northeastern United States, *J. Geophys.*](#)
678 [*Res. Atmos.*, 121, 10355–10376, <https://doi.org/10.1002/2016JD025311>, 2016.](#)

679 Guo, H., Weber, R. J., and Nenes, A.: High levels of ammonia do not raise fine particle pH
680 sufficiently to yield nitrogen oxide-dominated sulfate production, *Sci. Rep.*, 7, 12109, 2017.

681 Hallquist, M., Wenger, J. C., Baltensperger, U., Rudich, Y., Simpson, D., Claeys, M., Dommen,
682 J., Donahue, N. M., George, C., Goldstein, A. H., Hamilton, J. F., Herrmann, H., Hoffmann, T.,
683 Iinuma, Y., Jang, M., Jenkin, M. E., Jimenez, J. L., Kiendler-Scharr, A., Maenhaut, W.,
684 McFiggans, G., Mentel, Th. F., Monod, A., Prévôt, A. S. H., Seinfeld, J. H., Surratt, J. D.,
685 Szmigielski, R., and Wildt, J.: The formation, properties and impact of secondary organic
686 aerosol: current and emerging issues, *Atmos. Chem. Phys.*, 9, 5155–5236, <https://doi.org/10.5194/acp9-5155-2009>, 2009.

688 Halperin, J., and Taube, H.: The transfer of oxygen atoms in oxidation—reduction reactions. IV.
689 The reaction of hydrogen peroxide with sulfite and thiosulfate, and of oxygen, manganese
690 dioxide and of permanganate with sulfite, *J. Am. Chem. Soc.*, 74, 380–382, 1952.

691 Hanson, D. R., Ravishankara, A. R., and Solomon, S.: Heterogeneous reactions in sulfuric acid
692 aerosols: A framework for model calculations, *J. Geophys. Res.*, 99, 3615, <https://doi.org/10.1029/93JD02932>, 1994.

694 Hartz, K. E. H., Rosenorn, T., Ferchak, S. R., Raymond, T. M., Bilde, M., Donahue, N. M., and
695 Pandis, S. N.: Cloud condensation nuclei activation of monoterpene and sesquiterpene
696 secondary organic aerosol, *J. Geophys. Res.-Atmos.*, 110(D14), D14208, doi:10.1029/2004J
697 D005754, 2005.

698 He, L.-Y., Huang, X.-F., Xue, L., Hu, M., Lin, Y., Zheng, J., Zhang, R., and Zhang, Y.-H.:
699 Submicron aerosol analysis and organic source apportionment in an urban atmosphere
700 in Pearl River Delta of China using high-resolution aerosol mass spectrometry, *J. Geophys. Res.*
701 *Atmos.*, 116, D12304, <https://doi.org/10.1029/2010JD014566>, 2011.

702 Herrmann, H.: Kinetics of aqueous phase reactions relevant for atmospheric chemistry, *Chem.*
703 *Rev.*, 103, 4691–4716, 2003.

704 Hildebrandt, L., Donahue, N. M., Pandis, S. N.: High formation of secondary organic aerosol
705 from the photo-oxidation of toluene, *Atmos. Chem. Phys.*, 9, 2973–2986, <https://doi.org/10.5194/acp-9-2973-2009>, 2009.

706

707 Huang, L., An, J., Koo, B., Yarwood, G., Yan, R., Wang, Y., Huang, C., and Li, L.: Sulfate
708 formation during heavy winter haze events and the potential contribution from heterogeneous
709 SO₂ + NO₂ reactions in the Yangtze River Delta region, China, *Atmos. Chem. Phys.*, 19, 14311-
710 14328, 10.5194/acp-19-14311-2019, 2019.

711 Huang, L., Coddens, E. M., and Grassian, V. H.: Formation of organosulfur compounds from
712 aqueous phase reactions of S (IV) with methacrolein and methyl vinyl ketone in the presence of
713 transition metal ions, *ACS Earth Space Chem.*, 3, 1749-1755, 2019.

714 Huang, L., Liu, T. and Grassian, V. H.: Radical-initiated formation of aromatic organosulfates
715 and sulfonates in the aqueous phase. *Environ. Sci. Technol.*, 54, 11857–11864,
716 <https://doi.org/10.1021/acs.est.0c05644>, 2020.

717 Huang, R. J., Zhang, Y. L., Bozzetti, C., Ho, K. F., Cao, J. J., Han, Y. M., Daellenbach, K. R.,
718 Slowik, J. G., Platt, S. M., Canonaco, F., Zotter, P., Wolf, R., Pieber, S. M., Brun, E. A., Crippa,
719 M., Ciarelli, G., Piazzalunga, A., Schwikowski, M., Abbaszade, G., Schnelle-Kreis, J.,
720 Zimmermann, R., An, Z., Szidat, S., Baltensperger, U., Haddad, I. E., and Prevot, A. S. H.: High
721 secondary aerosol contribution to particulate pollution during haze events in China, *Nature*, 514,
722 218–222, 2014.

723 Huang, R. J., He, Y., Duan, J., Li, Y., Chen, Q., Zheng, Y., Chen, Y., Hu, W., Lin, C., Ni, H.,
724 Dai, W., Cao, J., Wu, Y., Zhang, R., Xu, W., Ovadnevaite, J., Ceburnis, D., Hoffmann, T., and
725 O'Dowd, C. D.: Contrasting sources and processes of particulate species in haze days with low
726 and high relative humidity in wintertime Beijing, *Atmos. Chem. Phys.*, 20, 9101-9114,
727 10.5194/acp-20-9101-2020, 2020.

728 [Hung, H. M. and Hoffmann, M. R.: Oxidation of gas-phase SO₂ on the surfaces of acidic
729 microdroplets: Implications for sulfate and sulfate radical anion formation in the atmospheric
730 liquid phase, *Environ. Sci. Technol.*, 49, 13768–13776, <https://doi.org/10.1021/acs.est.5b01658>,
731 2015.](#)

Formatted: Subscript

732 [Hung, H. M., Hsu, M. N., and Hoffmann, M. R.: Quantification of SO₂ oxidation on interfacial
733 surfaces of acidic micro-droplets: Implication for ambient sulfate formation, *Environ. Sci.
734 Technol.*, 52, 9079–9086, <https://doi.org/10.1021/acs.est.8b01391>, 2018.](#)

Formatted: Subscript

735 Jang, M., and Kamens, R. M.: Atmospheric secondary aerosol formation by heterogeneous
736 reactions of aldehydes in the presence of a sulfuric acid aerosol catalyst, *Environ. Sci. Technol.*,
737 35, 4758-4766, 10.1021/es010790s, 2001.

Formatted: Default Paragraph Font, Font: (Default)
Calibri, 11 pt, Font color: Text 1, Do not check spelling
or grammar

738 Jimenez, J. L., Canagaratna, M. R., Donahue, N. M., Prevot, A. S. H., Zhang, Q., Kroll, J. H.,
739 DeCarlo, P. F., Allan, J. D., Coe, H., Ng, N. L., Aiken, A. C., Docherty, K. S., Ulbrich, I. M.,
740 Grieshop, A. P., Robinson, A. L., Duplissy, J., Smith, J. D., Wilson, K. R., Lanz, V. A., Hueglin,
741 C., Sun, Y. L., Tian, J., Laaksonen, A., Raatikainen, T., Rautiainen, J., Vaattovaara, P., Ehn, M.,
742 Kulmala, M., Tomlinson, J. M., Collins, D. R., Cubison, M. J., Dunlea, J., Huffman, J. A.,
743 Onasch, T. B., Alfarra, M. R., Williams, P. I., Bower, K., Kondo, Y., Schneider, J., Drewnick,
744 F., Borrmann, S., Weimer, S., Demerjian, K., Salcedo, D., Cottrell, L., Griffin, R., Takami, A.,
745 Miyoshi, T., Hatakeyama, S., Shimono, A., Sun, J. Y., Zhang, Y. M., Dzepina, K., Kimmel,
746 J. R., Sueper, D., Jayne, J. T., Herndon, S. C., Trimborn, A. M., Williams, L. R., Wood, E. C.,
747 Middlebrook, A. M., Kolb, C. E., Baltensperger, U., and Worsnop, D. R.: Evolution of organic
748 aerosols in the atmosphere, *Science*, 326, 1525–1529, <https://doi.org/10.1126/science.1180353>,
749 2009.

750 Kautzman, K., Surratt, J., Chan, M., Chan, A., Hersey, S., Chhabra, P., Dalleska, N., Wennberg,
751 P., Flagan, R., and Seinfeld, J.: Chemical composition of gas-and aerosol-phase products from
752 the photooxidation of naphthalene, *J. Phys. Chem. A*, 114, 913-934, 2009.

753 Knipping, E. M., Lakin, M. J., Foster, K. L., Jungwirth, P., Tobias, D. J., Gerber, R. B., Dabdub,
754 D., and Finlayson-Pitts, B. J.: Experiments and simulations of ion-enhanced interfacial chemistry
755 on aqueous NaCl aerosols, *Science*, 288, 301, 10.1126/science.288.5464.301, 2000.

756 Krapf, M., El Haddad, I., Bruns, E. A., Molteni, U., Daellenbach, K. R., Prévôt, A. S.,
757 Baltensperger, U., and Dommen, J.: Labile peroxides in secondary organic aerosol, *Chem*, 1,
758 603-616, 2016.

759 Laskin, A., Gaspar, D. J., Wang, W., Hunt, S. W., Cowin, J. P., Colson, S. D., and Finlayson-
760 Pitts, B. J.: Reactions at interfaces as a source of sulfate formation in sea-salt particles, *Science*,
761 301, 340, 10.1126/science.1085374, 2003.

762 Leng, C. B., Roberts, J. E., Zeng, G., Zhang, Y. H., and Liu, Y.: Effects of temperature, pH, and
763 ionic strength on the Henry's law constant of triethylamine, *Geophys. Res. Lett.*, 42, 3569-3575,
764 10.1002/2015gl063840, 2015.

765 Li, G., Bei, N., Cao, J., Huang, R., Wu, J., Feng, T., Wang, Y., Liu, S., Zhang, Q., Tie, X., and
766 Molina, L. T.: A possible pathway for rapid growth of sulfate during haze days in China, *Atmos.*
767 *Chem. Phys.*, 17, 3301–3316, <https://doi.org/10.5194/acp17-3301-2017>, 2017.

768 Li, J., Zhang, Y., Cao, F., Zhang, W., Fan, M., Lee, X., Michalski, G.: Stable sulfur isotopes
769 revealed a major role of transition-metal-ion catalyzed SO₂ oxidation in haze episodes,
770 [doi:10.1021/acs.est.9b07150](https://doi.org/10.1021/acs.est.9b07150), 2020.

771 Lind, J. A., Lazrus, A. L., and Kok, G. L.: Aqueous phase oxidation of sulfur (IV) by hydrogen
772 peroxide, methylhydroperoxide, and peroxyacetic acid, *J. Geophys. Res. Atmos.*, 92, 4171-4177,
773 1987.

774 Liu, C., Chen, T., Liu, Y., Liu, J., He, H., Zhang, P.: Enhancement of secondary organic aerosol
775 formation and its oxidation state by SO₂ during photooxidation of 2-methoxyphenol, *Atmos.*
776 *Chem. Phys.*, 19, 2687-2700, 2019.

777 Liu, L., Bei, N., Wu, J., Liu, S., Zhou, J., Li, X., Yang, Q., Feng, T., Cao, J., Tie, X. and Li, G.:
778 Effects of stabilized Criegee intermediates (sCIs) on sulfate formation: a sensitivity analysis
779 during summertime in Beijing–Tianjin–Hebei (BTH), China, *Atmos. Chem. Phys.*, 19, 13341-
780 13354, 2019.

781 Liu, T., Clegg, S. L. and Abbatt, J. P. D.: Fast oxidation of sulfur dioxide by hydrogen peroxide
782 in deliquesced aerosol particles, *Proc. Natl. Acad. Sci. U. S. A.*, 117, 1354–1359, 2020.

783 Liu, Y., Liggio, J., Staebler, R., and Li, S. M.: Reactive uptake of ammonia to secondary organic
784 aerosols: kinetics of organonitrogen formation, *Atmos. Chem. Phys.*, 15, 13569–13584,
785 [doi:10.5194/acp-15-13569-2015](https://doi.org/10.5194/acp-15-13569-2015), 2015.

786 Maaß, F., Elias, H., and Wannowius, K. J.: Kinetics of the oxidation of hydrogen sulfite by
787 hydrogen peroxide in aqueous solution: ionic strength effects and temperature dependence,
788 *Atmos. Environ.*, 33, 4413-4419, [https://doi.org/10.1016/S1352-2310\(99\)00212-5](https://doi.org/10.1016/S1352-2310(99)00212-5), 1999.

789 Mauldin, R. L., Berndt, T., Sipilä, M., Paasonen, P., Petäjä, T., Kim, S., Kurtén, T., Stratmann,
790 F., Kerminen, V. M., and Kulmala, M.: A new atmospherically relevant oxidant of sulphur
791 dioxide, *Nature*, 488, 193–196, <https://doi.org/10.1038/nature11278>, 2012.

792 Mekic, M., Loisel, G., Zhou, W., Jiang, B., Vione, D., and Gligorovski, S.: Ionic-strength effects
793 on the reactive uptake of ozone on aqueous pyruvic acid: Implications for air–sea ozone
794 deposition, *Environ. Sci. Technol.*, 52, 12306–12315, 10.1021/acs.est.8b03196, 2018.

795 Mekic, M., Zeng, J., Zhou, W., Loisel, G., Jin, B., Li, X., Vione, D., and Gligorovski, S.: Ionic
796 strength effect on photochemistry of fluorene and dimethylsulfoxide at the air–sea interface:
797 Alternative formation pathway of organic sulfur compounds in a marine atmosphere, *ACS Earth
798 Space Chem.*, 4, 1029–1038, 10.1021/acsearthspacechem.0c00059, 2020.

799 Mishra, H., Enami, S., Nielsen, R. J., Hoffmann, M. R., Goddard, W. A., and Colussi, A. J.:
800 Anions dramatically enhance proton transfer through aqueous interfaces, *Proc. Natl. Acad. Sci.
801 U. S. A.*, 109, 10228–10232, 2012.

802 [Newland, M. J., Rickard, A. R., Vereecken, L., Muñoz, A., Ródenas, M., and Bloss, W. J.:](#)
803 [Atmospheric isoprene ozonolysis: impacts of stabilised Criegee intermediate reactions with SO₂,](#)
804 [H₂O and dimethyl sulfide, *Atmos. Chem. Phys.*, 15, 9521–9536, \[https://doi.org/10.5194/acp-15-\]\(https://doi.org/10.5194/acp-15-9521-2015\)](#)
805 [9521-2015, 2015.](#)

806 Ng, N., Kroll, J., Chan, A., Chhabra, P., Flagan, R., and Seinfeld, J.: Secondary organic aerosol
807 formation from m-xylene, toluene, and benzene, *Atmos. Chem. Phys.*, 7, 3909–3922,
808 <http://www.atmos-chem-phys.net/7/3909/2007/>, 2007.

809 Ng, N. L., Kwan, A. J., Surratt, J. D., Chan, A. W. H., Chhabra, P. S., Sorooshian, A., Pye, H. O.
810 T., Crouse, J. D., Wennberg, P. O., Flagan, R. C., and Seinfeld, J. H.: Secondary organic
811 aerosol (SOA) formation from reaction of isoprene with nitrate radicals (NO₃), *Atmos. Chem.
812 Phys.*, 8, 4117–4140, <http://www.atmos-chem-phys.net/8/4117/2008/>, 2008.

813 [Nguyen, T. B., Tyndall, G. S., Crouse, J. D., Teng, A. P., Bates, K. H., Schwantes, R. H.,](#)
814 [Coggon, M. M., Zhang, L., Feiner, P., Miller, D. O., Skog, K. M., Rivera-Rios, J. C., Dorris, M.,](#)
815 [Olson, K. F., Koss, A., Wild, R. J., Brown, S. S., Goldstein, A. H., de Gouw, J. A., Brune,](#)
816 [W. H., Keutsch, F. N., Seinfeld, J. H., and Wennberg, P. O.: Atmospheric fates of Criegee](#)
817 [intermediates in the ozonolysis of isoprene, *Phys. Chem. Chem. Phys.*, 18, 10 241–10 254,](#)
818 <https://doi.org/10.1039/C6CP00053C>, <http://dx.doi.org/10.1039/C6CP00053C>, 2016.

819 O'Brien, R. E., Wang, B., Kelly, S. T., Lundt, N., You, Y., Bertram, A. K., Leone, S. R., Laskin,
820 A., and Gilles, M. K.: Liquid–liquid phase separation in aerosol particles: Imaging at the
821 nanometer scale, *Environ. Sci. Technol.*, 49, 4995–5002, 10.1021/acs.est.5b00062, 2015.

822 Pankow, J. F. and Asher, W. E.: SIMPOL.1: a simple group contribution method for predicting
823 vapor pressures and enthalpies of vaporization of multifunctional organic compounds, *Atmos.
824 Chem. Phys.*, 8, 2773–2796, <http://www.atmos-chem-phys.net/8/2773/2008/>, 2008.

825 Qiu, J., Liang, Z., Tonokura, K., Colussi, A. J., and Enami, S.: Stability of monoterpene-derived
826 α -hydroxyalkyl-hydroperoxides in aqueous organic media – relevance to the fate of
827 hydroperoxides in aerosol particle phases, *Environ. Sci. Technol.*, 10.1021/acs.est.9b07497,
828 2020.

Formatted: Subscript

Formatted: Subscript

829 Rodríguez-Sevilla, J., Álvarez, M., Limiñana, G., Díaz, M. C.: Dilute SO₂ absorption equilibria
830 in aqueous HCl and NaCl solutions at 298.15 K, *J. Chem. Eng. Data*, 47, 1339-1345, 2002.

831 Ruiz-Lopez, M.F., Francisco, J.S., Martins-Costa, M.T. and Anglada, J.M.: Molecular reactions
832 at aqueous interfaces. *Nat. Rev. Chem.*, 1-17, 2020.

833 Seinfeld, J. H., and Pandis, S. N.: *Atmospheric chemistry and physics: from air pollution to*
834 *climate change*, John Wiley & Sons, 2012.

835 Sha, T., Ma, X., Jia, H., Tian, R., Chang, Y., Cao, F., and Zhang, Y.: Aerosol chemical
836 component: Simulations with WRF-Chem and comparison with observations in Nanjing, *Atmos.*
837 *Environ.*, 218, 116982, <https://doi.org/10.1016/j.atmosenv.2019.116982>, 2019.

838 Shang, J., Li, J., Zhu, T.: Heterogeneous reaction of SO₂ on TiO₂ particles. *Sci. China Chem.*, 53,
839 2637–2643, 2010.

840 Shi, Q., Davidovits, P., Jayne, J. T., Worsnop, D. R., and Kolb, C. E.: Uptake of gas-phase
841 ammonia. 1. Uptake by aqueous surfaces as a function of pH, *J. Phys. Chem. A*, 103, 8812-8823,
842 10.1021/jp991696p, 1999.

843 Song, M., Marcolli, C., Krieger, U. K., Zuend, A., and Peter, T.: Liquid–liquid phase separation
844 in aerosol particles: dependence on O:C, organic functionalities, and compositional complexity,
845 *Geophys. Res. Lett.*, 39, L19801, doi:10.1029/2012GL052807, 2012.

846 Song, S., Gao, M., Xu, W., Shao, J., Shi, G., Wang, S., Wang, Y., Sun, Y., and McElroy, M. B.:
847 Fine-particle pH for Beijing winter haze as inferred from different thermodynamic equilibrium
848 models, *Atmos. Chem. Phys.*, 18, 7423–7438, <https://doi.org/10.5194/acp-18-7423-2018>, 2018.

849 Song, S., Gao, M., Xu, W., Sun, Y., Worsnop, D. R., Jayne, J. T., Zhang, Y., Zhu, L., Li, M.,
850 Zhou, Z., Cheng, C., Lv, Y., Wang, Y., Peng, W., Xu, X., Lin, N., Wang, Y., Wang, S., Munger,
851 J. W., Jacob, D. J., and McElroy, M. B.: Possible heterogeneous chemistry of hydroxy
852 methanesulfonate (HMS) in northern China winter haze, *Atmos. Chem. Phys.*, 19, 1357–1371,
853 <https://doi.org/10.5194/acp-19-1357-2019>, 2019.

854 Su, H., Cheng, Y., and Poschl, U.: New multiphase chemical processes influencing atmospheric
855 aerosols, air quality, and climate in the anthropocene, *Acc. Chem. Res.*, e1601530-2983,
856 <https://doi.org/10.1021/acs.accounts.0c00246>, 2020.

857 Sun, Y., Wang, Z., Fu, P., Jiang, Q., Yang, T., Li, J., and Ge, X.: The impact of relative humidity
858 on aerosol composition and evolution processes during wintertime in Beijing, China, *Atmos.*
859 *Environ.*, 77, 927-934, 2013.

860 Surratt, J. D., Murphy, S. M., Kroll, J. H., Ng, N. L., Hildebrandt, L., Sorooshian, A.,
861 Szmigielski, R., Vermeylen, R., Maenhaut, W., and Claeys, M.: Chemical composition of
862 secondary organic aerosol formed from the photooxidation of isoprene, *J. Phys. Chem. A*, 110,
863 9665-9690, 2006.

864 Thornton, J. A., Braban, C. F., and Abbatt, J. P. D.: N₂O₅ hydrolysis on sub-micron organic
865 aerosols: the effect of relative humidity, particle phase, and particle size, *Phys. Chem. Chem*
866 *Phys.*, 5, 4593–4603, <https://doi.org/10.1039/B307498F>, 2003.

867 Tie, X., Brasseur, G., Emmons, L., Horowitz, I., and Kinnison, D.: Effects of aerosols on
868 tropospheric oxidants: a global model study, *J. Geophys. Res. Atmos.*, 106, 22931–22964, 2001.

869 [Tong, H., Arangio, A. M., Lakey, P. S. J., Berkemeier, T., Liu, F., Kampf, C. J., Brune, W. H.,](#)
870 [Pöschl, U., and Shiraiwa, M.: Hydroxyl radicals from secondary organic aerosol decomposition](#)
871 [in water, *Atmos. Chem. Phys.*, 16, 1761–1771, doi:10.5194/acp-16-1761-2016, 2016.](#)

872 Usher, C. R., Al-Hosney, H., Carlos-Cuellar, S., and Grassian, V. H.: A laboratory study of the
873 heterogeneous uptake and oxidation of sulfur dioxide on mineral dust particles, *J. Geophys. Res.*,
874 107, 4713, doi:10.1029/2002JD002051, 2002.

875 Varutbangkul, V., Brechtel, F. J., Bahreini, R., Ng, N. L., Keywood, M. D., Kroll, J. H., Flagan,
876 R. C., Seinfeld, J. H., Lee, A., and Goldstein, A. H.: Hygroscopicity of secondary organic
877 aerosols formed by oxidation of cycloalkenes, monoterpenes, sesquiterpenes, and related
878 compounds, *Atmos. Chem. Phys.*, 6, 2367–2388, [http://www.atmos-chem-phys.net/6/23](http://www.atmos-chem-phys.net/6/2367/2006/)
879 [67/2006/](http://www.atmos-chem-phys.net/6/2367/2006/), 2006.

880 Veghte, D. P., Altaf, M. B., and Freedman, M. A.: Size dependence of the structure of organic
881 aerosol, *J. Am. Chem. Soc.*, 135, 16046–16049, 2013.

882 Wang, G., Zhang, R., Gomez, M. E., Yang, L., Zamora, M. L., Hu, M., Lin, Y., Peng, J., Guo, S.,
883 and Meng, J.: Persistent sulfate formation from London Fog to Chinese haze, *Proc. Natl. Acad.*
884 *Sci. U. S. A.*, 113, 13630–13635, 2016.

885 Wang, S., Ye, J., Soong, R., Wu, B., Yu, L., Simpson, A. J., and Chan, A. W. H.: Relationship
886 between chemical composition and oxidative potential of secondary organic aerosol from
887 polycyclic aromatic hydrocarbons, *Atmos. Chem. Phys.*, 18, 3987–4003, 2018.

888 Wang, S., Zhou, S., Tao, Y., Tsui, W. G., Ye, J., Yu, J. Z., Murphy, J. G., McNeill, V. F.,
889 Abbatt, J. P. D., and Chan, A. W. H.: Organic peroxides and sulfur dioxide in aerosol: Source of
890 particulate sulfate, *Environ. Sci. Technol.*, 53, 10695–10704, 10.1021/acs.est.9b02591, 2019.

891 Wang, X.; Gemayel, R.; Hayeck, N.; Perrier, S.; Charbonnel, N.; Xu, C.; Chen, H.; Zhu, C.;
892 Zhang, L.; Wang, L.; Nizkorodov, S. A.; Wang, X.; Wang, Z.; Wang, T.; Mellouki, A.; Riva, M.;
893 Chen, J.; George, C. Atmospheric photosensitization: A new pathway for sulfate formation,
894 *Environ. Sci. Technol.*, 54, 3114–3120, 2020.

895 Wang, Y., Zhang, Q., Jiang, J., Zhou, W., Wang, B., He, K., Duan, F., Zhang, Q., Philip, S., and
896 Xie, Y.: Enhanced sulfate formation during China's severe winter haze episode in January 2013
897 missing from current models, *J. Geophys. Res. Atmos.*, 119, 10425–10440,
898 <https://doi.org/10.1002/2013JD021426>, 2014.

899 Wei, H., Vejerano, E. P., Leng, W., Huang, Q., Willner, M. R., Marr, L. C., and Vikesland, P. J.:
900 Aerosol microdroplets exhibit a stable pH gradient, *Proc. Natl. Acad. Sci. U. S. A.*, 115, 7272,
901 10.1073/pnas.1720488115, 2018.

902 Xu, L., Guo, H., Boyd, C. M., Klein, M., Bougiatioti, A., Cerully, K. M., Hite, J. R., Isaacman-
903 VanWertz, G., Kreisberg, N. M., and Knote, C.: Effects of anthropogenic emissions on aerosol
904 formation from isoprene and monoterpenes in the southeastern United States, *Proc. Natl. Acad.*
905 *Sci. U. S. A.*, 112, 37–42, 2015.

906 Yang, Y., Wang, H., Smith, S. J., Easter, R., Ma, P.-L., Qian, Y., Yu, H., Li, C., and Rasch, P. J.:
907 Global source attribution of sulfate concentration and direct and indirect radiative forcing,
908 *Atmos. Chem. Phys.*, 17, 8903–8922, <https://doi.org/10.5194/acp17-8903-2017>, 2017.

909 Yao, M., Zhao, Y., Hu, M., Huang, D., Wang, Y.C., Yu, J. Z., and Yan, N.: Multiphase reactions
910 between secondary organic aerosol and sulfur dioxide: kinetics and contributions to sulfate
911 formation and aerosol aging, *Environ. Sci. Tech. Let.* 6, 768-774, 10.1021/acs.estlett.9b00657,
912 2019.

913 Ye, J., Gordon, C. A., and Chan, A. W. H: Enhancement in secondary organic aerosol formation
914 in the presence of preexisting organic particle, *Environ. Sci. Technol.*, 50, 3572-3579, 2016.

915 Ye, J., Abbatt, J. P. D., and Chan, A. W. H.: Novel pathway of SO₂ oxidation in the atmosphere:
916 reactions with monoterpene ozonolysis intermediates and secondary organic aerosol, *Atmos.*
917 *Chem. Phys.*, 18, 5549–5565, <https://doi.org/10.5194/acp18-5549-2018>, 2018.

918 Yee, L. D., Isaacman-VanWertz, G., Wernis, R. A., Kreisberg, N. M., Glasius, M., Riva, M.,
919 Surratt, J. D., de Sá, S. S., Martín, S. T., Alexander, M. L., Palm, B. B., Hu, W., Campuzano-
920 Jost, P., Day, D. A., Jimenez, J. L., Liu, Y., Misztal, P. K., Artaxo, P., Viegas, J., Manzi, A., de
921 Souza, R. A. F., Edgerton, E. S., Baumann, K., and Goldstein, A. H.: Natural and
922 anthropogenically influenced isoprene oxidation in southeastern United States and central
923 Amazon, *Environ. Sci. Technol.*, 54, 5980-5991, 10.1021/acs.est.0c00805, 2020.

924 You, Y., Renbaum-Wolff, L., Bertram, A. K: Liquid-liquid phase separation in particles
925 containing organics mixed with ammonium sulfate, ammonium bisulfate, ammonium nitrate or
926 sodium chloride, *Atmos. Chem. Phys.*, 13, 11723–11734, [https://doi.org/10.5194/acp-13-11723-](https://doi.org/10.5194/acp-13-11723-2013)
927 2013, 2013.

928 You, Y., Smith, M. L., Song, M., Martin, S. T., and Bertram, A. K.: Liquid–liquid phase
929 separation in atmospherically relevant particles consisting of organic species and inorganic salts,
930 *Int. Rev. Phys. Chem.*, 33, 43–77, doi:10.1080/0144235X.2014.890786, 2014.

931 Zhang, S., Xing, J., Sarwar, G., Ge, Y., He, H., Duan, F., Zhao, Y., He, K., Zhu, L. and Chu, B.:
932 Parameterization of heterogeneous reaction of SO₂ to sulfate on dust with coexistence of NH₃
933 and NO₂ under different humidity conditions, *Atmos. Environ.*, 208, 133-140, 2019.

934 Zhao, Y., Liu, Y., Ma, J., Ma, Q., and He, H.: Heterogeneous reaction of SO₂ with soot: The
935 roles of relative humidity and surface composition of soot in surface sulfate formation, *Atmos.*
936 *Environ.*, 152, 465-476, 2017.

937 Zheng, B., Zhang, Q., Zhang, Y., He, K. B., Wang, K., Zheng, G. J., Duan, F. K., Ma, Y. L., and
938 Kimoto, T.: Heterogeneous chemistry: a mechanism missing in current models to explain
939 secondary inorganic aerosol formation during the January 2013 haze episode in North China,
940 *Atmos. Chem. Phys.*, 15, 2031–2049, doi:10.5194/acp-15-2031-2015, 2015.

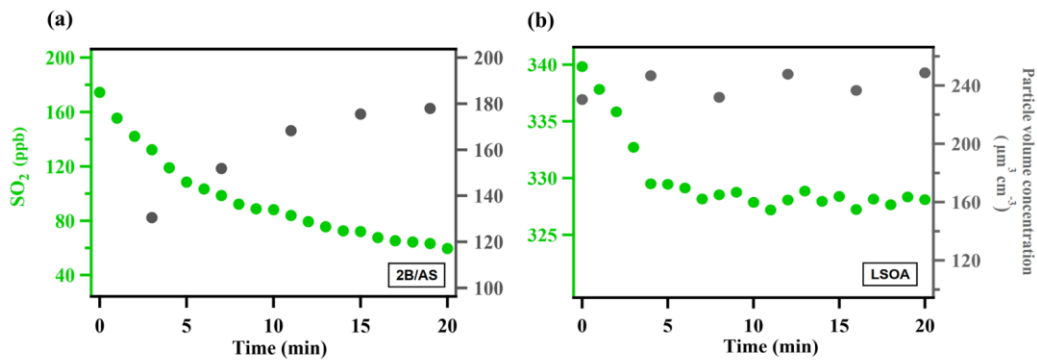
941 Zheng, G. J., Duan, F. K., Su, H., Ma, Y. L., Cheng, Y., Zheng, B., Zhang, Q., Huang, T.,
942 Kimoto, T., Chang, D., Pöschl, U., Cheng, Y. F., and He, K. B.: Exploring the severe winter haze
943 in Beijing: the impact of synoptic weather, regional transport and heterogeneous reactions,
944 *Atmos. Chem. Phys.*, 15, 2969–2983, doi:10.5194/acp-15-2969-2015, 2015.

945

946

947

948



949

950 **Figure 1.** Typical evolution of the species monitored during γ_{SO_2} measurement for (a)
 951 ammonium sulfate mixed with 2-butanone organic peroxide (2B/AS, Expt. 16) and (b) limonene
 952 SOA (LSOA, Expt. 27). Particle volume concentrations measured by SMPS have been corrected
 953 for wall loss assuming a pseudo first-order loss rate (Ye et al., 2016). γ_{SO_2} was calculated for the
 954 initial portion of the decay (first 7 minutes).

955

956

957

958

959

960

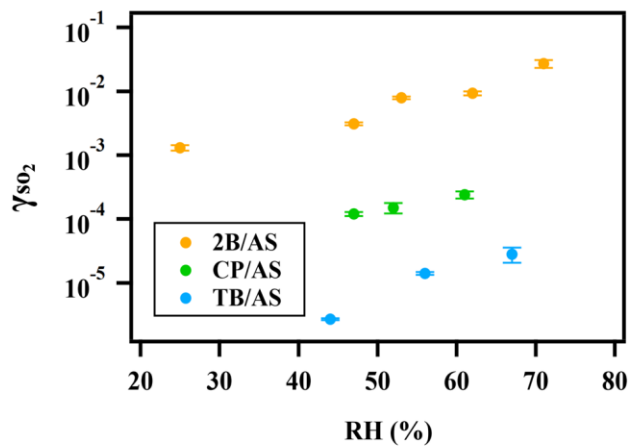
961

962

963

964

965



966
967 **Figure 2.** Exponential relationship between γ_{SO_2} and RH for ammonium sulfate aerosol
968 containing 2-butanone peroxide (2B), cumene hydroperoxide (CP), tert-butyl hydroperoxide
969 (TB).

970

971

972

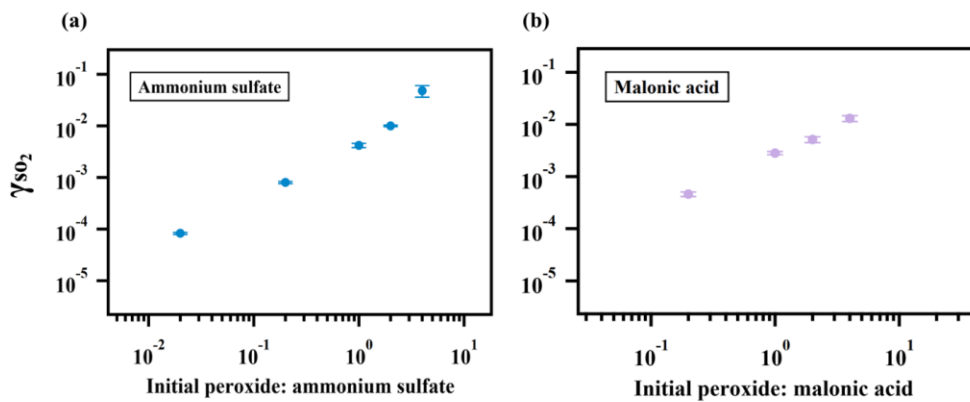
973

974

975

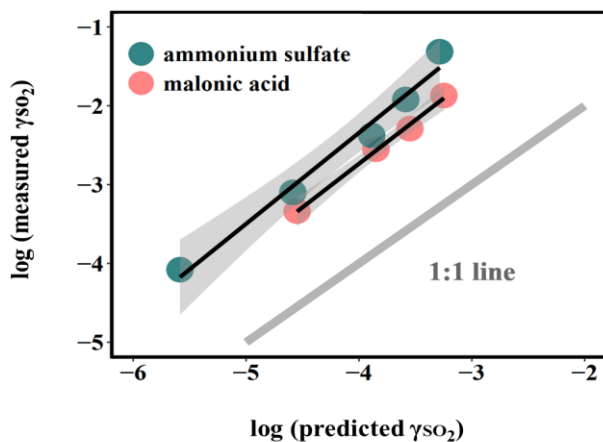
976

977



978
 979 **Figure 3.** Relationship between γ_{SO_2} and particulate peroxide content. γ_{SO_2} for ammonium sulfate
 980 (a) and malonic acid aerosol (b) containing different amount of 2-butanone peroxide are shown
 981 here. The observed dependence of γ_{SO_2} on the amount of peroxide injected are linear since the
 982 slopes of the relationship are both nearly 1 in (a) and (b).

983
 984
 985
 986
 987
 988
 989



990

991 **Figure 4.** Relationship between measured γ_{SO_2} and γ_{SO_2} predicted by Eqn. 4. The large deviation

992 from the 1:1 line, which represents the difference between the measured uptake coefficient and

993 predicted values based on kinetics in the dilute aqueous phase, indicates that aerosol reactive

994 uptake is significantly faster than reactions in dilute aqueous phase. This enhancement is likely

995 driven in part by high ionic strengths, as the difference between measured γ_{SO_2} and predicted γ_{SO_2}

996 are consistently higher for organic peroxide containing ammonium sulfate (high ionic strength)

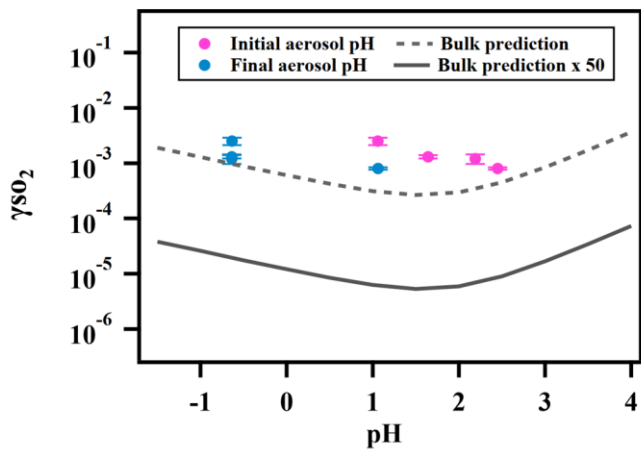
997 than for that mixed with malonic acid (lower ionic strength).

998

999

1000

1001



1002

1003 **Figure 5.** Relationship between γ_{SO_2} and aerosol phase pH for ammonium sulfate aerosol
 1004 containing 2-butanone peroxide.

1005

1006

1007

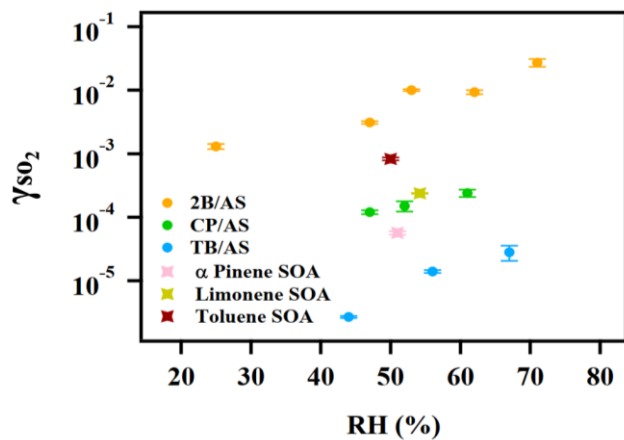
1008

1009

1010

1011

1012



1013

1014 **Figure 6.** γ_{SO_2} measured for different types of organic aerosol. The reactive uptake coefficient of
 1015 SO_2 onto SOA are on the order of 10^{-4} .

1016

1017

1018

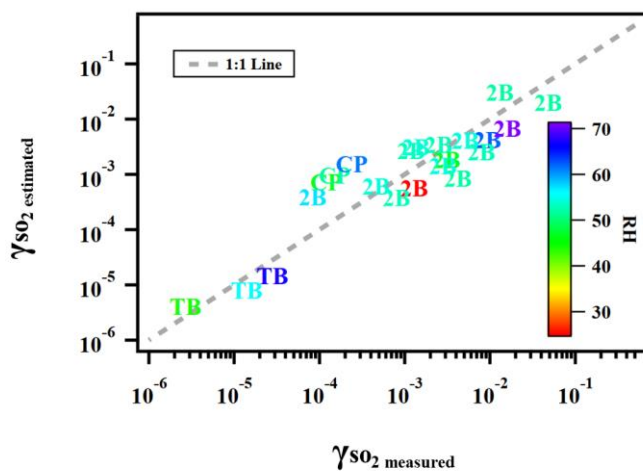
1019

1020

1021

1022

1023



1024

1025 **Figure 7.** Predicted γ_{SO_2} using Equation (8) versus measured γ_{SO_2} for ammonium sulfate or
 1026 malonic acid aerosol containing 2-butanone peroxide (2B), cumene hydroperoxide (CP), tert-
 1027 butyl hydroperoxide (TB) under different experimental conditions.

1028

1029

1030

1031

1032

1033

1034